Inorg. Chem. **2007**, *46*, 3367–3377

A New Chiral N,N′,O-Donor Heteroscorpionate Ligand. Structures of Ni^{2+}, Cu^{2+}, Zn^{2+} Complexes and Study of Solution Equilibria by Means of ^1H NMR/UV–Vis Titrations and EXSY NMR Spectroscopy

Marcello Gennari, Matteo Tegoni, Maurizio Lanfranchi, Maria Angela Pellinghelli, and Luciano Marchiò*

Dipartimento di Chimica Generale ed Inorganica, Chimica Analitica, Chimica Fisica, Universitá degli Studi di Parma, via Usberti 17/a, I 43100 Parma, Italy

Received November 23, 2006

The N,N′,O-heteroscorpionate ligand 1-(4-methoxy-3,5-dimethyl-pyridin-2-yl)-2-methyl-1-pyrazol-1-yl-propan-2-ol (LOH) was prepared in two high-yield steps. Complexes $[M(LOH)_2][MCl_4]$ (M^{2+} = Cu^{2+} and Zn^{2+}) and $[M(LOH)_2]Cl_2$ (M^{2+} = Ni^{2+} and Cu^{2+}) were prepared and characterized by X-ray crystallography. The speciation in solution (methanol:water 95:5) of the M^{2+}/LOH systems was investigated by means of spectrophotometric (Ni^{2+} and Cu^{2+}) and ^1H NMR (Zn^{2+}) titrations. The β_1 and β_2 global formation constants for the $[M(LOH)]^{2+}$ and $[M(LOH)_2]^{2+}$ species were obtained and are in agreement with the Irving–Williams series: Ni^{2+}< Cu^{2+}> Zn^{2+}. The Zn^{2+}/LOH system was studied by means of quantitative ^1H–^1H EXSY spectroscopy (300 K, mixing time = 0.2–0.8 s), which allows the description of the equilibria occurring between five octahedral $[Zn(LOH)_2]^{2+}$ structural isomers and tetrahedral [Zn-(LOH)Cl]Cl species. Exchange constants k_{ij}^{ex} and associated rate constants k_{ij} suggest that two types of interconversion occur: octahedral–octahedral (faster) and octahedral–tetrahedral (slower). DFT calculations (B3LYP/6-311+G(d)) were employed to evaluate the relative stability of the $[Zn(LOH)_2]^{2+}$ isomers, which are comparable for the five complexes with a maximum energy difference of 6.3 kJ/mol.

1. Introduction

Scorpionates are tripodal ligands which preferably link to metal ions by occupying a trigonal face of a coordination polyhedron.[1] A special category of scorpionate ligands is represented by heteroscorpionates,[2] which are characterized by at least two nonequivalent donor groups. In particular, the N,N,O-donor heteroscorpionates have found application in biomimetics, as synthetic models of the 2-Hys-1-carboxylate triad, which is present in various metalloproteins and metalloenzimes (mainly containing Zn and Fe but also Mn, Ni, and Cu),[3] in catalysis (Ti, Zr, Ru, Mo, and Al complexes),[4] and, more recently, as models for radiopharmaceu-

* To whom correspondence should be addressed. E-mail: marchio@unipr.it.

(1) (a) Trofimenko, S. *J. Am. Chem. Soc.* **1970**, *92*, 5118−5126. (b) Trofimenko, S. *Chem. Rev.* **1993**, *93*, 943−980. (c) Trofimenko, S. *Polyhedron* **2004**, *23*, 197−203. (d) Edelman, F. T. *Angew. Chem., Int. Ed.* **2001**, *40*, 1656−1660. (e) Pettinari, C.; Pettinari, R. *Coord. Chem. Rev.* **2005**, *249*, 525−543. (f) Pettinari, C.; Pettinari, R. *Coord. Chem. Rev.* **2005**, *249*, 663−691.

(2) (a) Otero, A; Fernández Baeza, J.; Antiñolo, A.; Tejeda, J.; Lara-Sánchez, A. *Dalton Trans.* **2004**, 1499−1510. (b) Higgs, T. C.; Carrano, C. J. *Inorg. Chem.* **1997**, *36*, 291−297. (c) Higgs, T. C.; Ji, D.; Czernuszewicz, R. S.; Matzanke, B. F.; Schunemann, V.; Trautwein, A. X.; Helliwell, M.; Ramirez, W.; Carrano, C. J. *Inorg. Chem.* **1998**, *37*, 2383−2392. (d) Klimbin, C.; Hascall, T.; Parkin, G. *Inorg. Chem.* **1997**, *36*, 5680−5681. (e) Ghosh, P.; Parkin, G. *Chem. Commun.* **1998**, 413−414. (f) Trösh, A.; Vahrenkamp, H. *Eur. J. Inorg. Chem.* **1998**, 827−832. (g) Karambelkar, V. V.; Krishnamurthy, D.; Stern, C. L.; Zakharov, L. N.; Rheingold, A. L.; Goldberg, D. P. *Chem. Commun.* **2002**, 2772−2773.

(3) (a) Dowling, C.; Parkin, G. *Polyhedron* **1996**, *15*, 2463−2465. (b) Ghosh, P.; Parkin, G. *Dalton. Trans.* **1998**, 2281−2283. (c) Hammes, B. S.; Carrano, C. J. *Inorg. Chem.* **1999**, *38*, 4593−4600. (d) Kail, B.; Nemykin, V. N.; Davie, S. R.; Carrano, C. J.; Hammes, B.; Basu, P. *Inorg. Chem.* **2002**, *41*, 1281−1291. (e) Hammes, B. S.; Kieber-Emmons, M. T.; Letizia, J. A.; Shirin, Z.; Carrano, C. J.; Zakharov, L. N.; Rheingold, A. L. *Inorg. Chim. Acta.* **2003**, 227−238. (f) Hammes, B. S.; Chohan, B. S.; Hoffman, J. T.; Einwachter, S.; Carrano, C. J. *Inorg. Chem.* **2004**, *43*, 7800−7806. (g) Beck, A.; Burzlaff, N.; Weibert, B. *Eur. J. Inorg. Chem.* **2001**, 521−527. (h) Barth, A.; Hübner, E.; Burzlaff, N. *Inorg. Chem.* **2003**, *42*, 7182−7188. (i) Hegelmann, I.; Beck, A.; Eichhorn, C.; Weibert, B.; Burzlaff, N. *Eur. J. Inorg. Chem.* **2003**, 339−347. (l) Müller, R.; Hübner, E.; Burzlaff, N. *Eur. J. Inorg. Chem.* **2004**, 2151−2159. (m) Bruijnincx, P. C. A.; Lutz, M.; Spek, A. L.; Van Faassen, E. E.; Weckhuysen, B. M.; Van Koten, G.; Klein Gebbink, R. J. M. *Eur. J. Inorg. Chem.* **2005**, 779−787.

(4) (a) Otero, A.; Fernández-Baeza, F.; Antiñolo, A.; Carrillo-Hermosilla, F.; Tejeda, J.; Díez-Barra, E.; Lara-Sánchez, A.; Sánchez-Barba, L.; López-Solera, I. *Organometallics* **2001**, *20*, 2428−2430. (b) Milione, S.; Montefusco, C.; Cuenca, T.; Grassi, A. *Chem. Commun.* **2003**,

10.1021/ic062228e CCC: $37.00
Published on Web 03/17/2007

Scheme 1. Different Classes of N,N,O-Donor Ligands

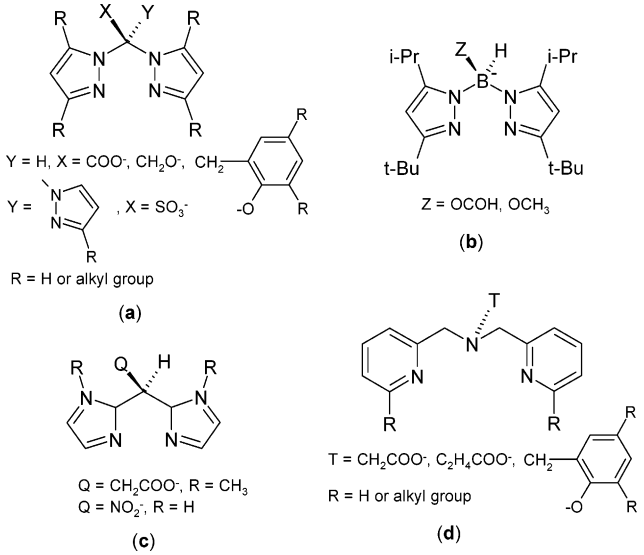

ticals (Re complexes).[5] As far as the topology of the ligands is concerned, N,N,O-heteroscorpionates can be grouped in three categories: (1) C-centric pyrazole-based, such as the bis(pyrazol-1-yl)-acetates,[3e,g,h,6] bis(pyrazol-1-yl)-ethoxydes,[7] bis(pyrazolyl)-phenolates,[2b,3c,8] and tris(pyrazol-1-yl)methane sulfonates[9] (Scheme 1a); (2) B-centric bis(pyrazol-1-yl)borato derivatives $(HCO_2)Bp$ and $(MeO)Bp$[3a,3b] (Scheme 1b); and (3) C-centric imidazole-based bis(imidazol-2-yl)propionates[3m] and bis(imidazol-2-yl)nitromethane[10] (Scheme 1c). An additional class is represented by N-centric tripodal ligands in which the bridging nitrogen atom is able to coordinate

Scheme 2

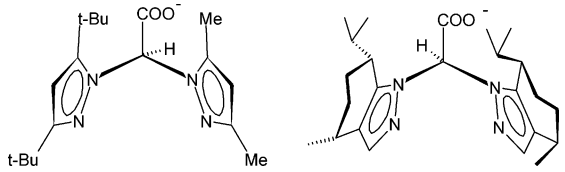

Scheme 3

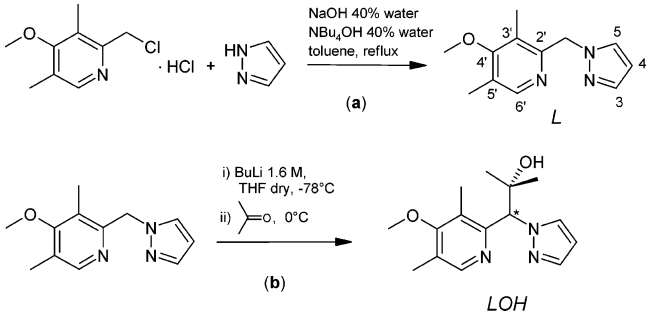

together with the N,N,O-donor set so that these ligands can be considered as N_3O tetradentate[11] (Scheme 1d).

Some N,N,O-heteroscorpionate ligands are chiral. The asymmetry is usually introduced by (1) employing three different donor groups connected to the central atom[3i,12] or (2) using an enantiopure heterocycle (e.g., camphorpyrazole or menthylpyrazole) as a precursor to yield a Hc^*_2AX ligand (Hc^* = enantiopure heterocycle, A = bridging atom, X = O-donor group), Scheme 2.[13] It is of note that only the latter method yields a homochiral ligand without complex enantiomeric/diastereoisomeric separations.

This work reports the synthesis of a new chiral pyrazolyl−pyridine-based N,N′,O-scorpionate ligand (LOH, Scheme 3). LOH can be prepared in two high-yield steps even though the reaction is not stereoselective (racemic mixture). This synthetic pathway first generates a prochiral N,N′ bidentate ligand, which can be opportunely functionalized on the methylene bridge by applying the synthetic procedures developed for derivatization of the bis(pyrazolyl)methanes.[2a]

The coordination properties of LOH were explored by reacting it with Ni^{2+}, Cu^{2+}, and Zn^{2+} in 1:1 and 1:2 M:LOH ratios. The X-ray single-crystal structures of the $[M(LOH)_2]Cl_2$ (M^{2+} = Cu^{2+} and Ni^{2+}) and $[M(LOH)_2][MCl_4]$ (M^{2+} = Cu^{2+} and Zn^{2+}) complexes show that the ligand is always κ^3-N,N′,O-coordinated. The speciation of the M^{2+}/LOH systems in methanol:water (95:5) was investigated by UV−vis (Ni^{2+} and Cu^{2+}) and ^1H NMR (Zn^{2+}) titrations. A detailed structural description of the Zn^{2+}/LOH system in solution was performed by means of ESI-MS, $^1H-^1H$ EXSY NMR spectroscopy, and DFT calculations.

2. Experimental Section

General Procedures. All reagents and solvents, except for THF (distilled from sodium benzophenone), were used as purchased from

1176−1177. (c) Milione, S.; Bertolasi, V.; Cuenca, T.; Grassi, A. *Organometallics* **2005**, *24*, 4915−4925. (d) Milione, S.; Grisi, F.; Centore, R.; Tuzi, A. *Organometallics* **2006**, *25*, 266−274. (e) Kopf, H.; Pietraszuk, C.; Hübner, E.; Burzlaff, N. *Organometallics* **2006**, *25*, 2533−2546. (f) Hoffman, J. T.; Tran, B. L.; Carrano, C. J. *Dalton Trans.* **2006**, 3822−3830.

(5) (a) Porchia, M.; Papini, G.; Santini, C.; Gioia Lobbia, G.; Pellei, M.; Tisato, F.; Bandoli, G.; Dolmella, A. *Inorg. Chem.* **2005**, *44*, 4045−4054. (b) Porchia, M.; Papini, G.; Santini, C.; Lobbia, G. G.; Pellei, M.; Tisato, F.; Bandoli, G.; Dolmella, A. *Inorg. Chim. Acta* **2006**, *359*, 2501−2508.

(6) (a) Otero, A.; Fernández-Baeza, J.; Tejeda, J.; Antiñolo, A.; Carrillo-Hermosilla, F.; Díez-Barra, E.; Lara-Sánchez, A.; Fernández-López, M.; Lanfranchi, M.; Pellinghelli, M. A. *Dalton Trans.* **1999**, 3537−3539. (b) Otero, A.; Fernández-Baeza, J.; Antiñolo, A.; Tejeda, J.; Lara-Sánchez, A.; Sánchez-Barba, L.; Rodríguez, A. M. *Dalton Trans.* **2004**, 3963−3969. (c) Otero, A.; Fernández-Baeza, J.; Tejeda, J.; Antiñolo, A.; Lara-Sánchez, A.; Sánchez-Barba, L.; Martinez-Caballero, E.; Rodríguez, A. M.; López-Solera, I. *Inorg. Chem.* **2005**, *44*, 5336−5344. (d) Burzlaff, N.; Hegelmann, I.; Weibert, B. *J. Organomet. Chem.* **2001**, *626*, 16−23.

(7) (a) Otero, A.; Fernández-Baeza, F.; Tejeda, J.; Antiñolo A.; Carrillo-Hermosilla, F.; Díez-Barra, E.; Lara-Sánchez, A.; Fernández-López, M. *Dalton Trans.* **2000**, 2367−2374. (b) Otero, A.; Fernández-Baeza, F.; Antiñolo A.; Tejeda, J.; Lara-Sánchez, A.; Sánchez-Barba, L.; Rodríguez, A. M. *Eur. J. Inorg. Chem.* **2004**, 260−266.

(8) (a) Higgs, T. C.; Carrano, C. J. *Inorg. Chem.* **1997**, *36*, 298−306. (b) Higgs, T. C.; Spartalian, K.; O'Connor, C. J.; Matzanke, B. F.; Carrano, C. J. *Inorg. Chem.* **1998**, *37*, 2263−2272. (c) Hammes, B. S.; Carrano, C. J. *Inorg. Chem.* **1999**, *38*, 3562−3568.

(9) (a) Kläui, W.; Berghahn, M.; Rheinwald, G.; Lang, H. *Angew. Chem., Int. Ed.* **2000**, *39*, 2464−2466. (b) Klaüi, W.; Schramm, D.; Peters, W.; Rheinwald, G.; Lang, H. *Eur. J. Inorg. Chem.* **2001**, 1415−1424. (c) Kläui, W.; Berghahn, M.; Frank, W.; Reiβ, G. J.; Schönherr, T.; Rheinwald, G.; Lang, H. *Eur. J. Inorg. Chem.* **2003**, 2059−2070. (d) Papish, E. T.; Taylor, M. T.; Jernigan III, F. E.; Rodig, M. J.; Shawhan, R. R.; Yap, G. P. A.; Jove, F. A. *Inorg. Chem.* **2006**, *45*, 2242−2250.

(10) Joseph, M.; Leigh, T.; Swain, M. L. *Synthesis* **1977**, *7*, 459−461.

(11) (a) Abufarag, A.; Vahrenkamp, H. *Inorg. Chem.* **1995**, *34*, 2207−2216. (b) Gross, F.; Vahrenkamp, H. *Inorg. Chem.* **2005**, *44*, 3321−3329.

(12) Otero, A.; Fernández-Baeza, J.; Antiñolo, A.; Tejeda, J.; Lara-Sánchez, A.; Sánchez-Barba, L.; Expósito, M. T.; Rodríguez, A. M. *Dalton Trans.* **2003**, 1614−1619.

(13) (a) Hegelmann, I.; Burzlaff, N. *Eur. J. Inorg. Chem.* **2003**, 409−411. (b) Peters, L.; Burzlaff, N. *Polyhedron* **2004**, 245−251.

Table 1. Summary of X-ray Crystallographic Data for **LOH**, **2a**, **3a**, **4a**, and **5a**[a]

	LOH	2a	3a	4a	5a
empirical formula	$C_{15}H_{21}N_3O_2$	$C_{33}H_{54}Cl_2N_6NiO_7$	$C_{32}H_{48}Cl_4Cu_2N_6O_6$	$C_{30}H_{46}Cl_2CuN_6O_6$	$C_{34}H_{48}Cl_4N_8O_4Zn_2$
fw	275.35	776.43	881.64	721.17	905.34
color, habit	colorless, block	violet, block	green, block	blue, plate	colorless, block
cryst size, mm	0.45 × 0.45 × 0.35	0.55 × 0.50 × 0.50	0.50 × 0.45 × 0.30	0.45 × 0.25 × 0.10	0.25 × 0.20 × 0.17
cryst syst	triclinic	monoclinic	monoclinic	orthorhombic	monoclinic
space group	$P\bar{1}$	$P2_1/n$	$C2/c$	Pbca	$C2/c$
a, Å	8.515(1)	11.3780(1)	25.631(2)	14.037(8)	26.383(3)
b, Å	10.540(2)	15.3700(1)	8.455(1)	18.297(6)	9.016(2)
c, Å	10.582(2)	11.4960(1)	21.883(2)	13.928(8)	22.609(2)
α, deg	63.298(2)	90	90	90	90
β, deg	86.374(2)	102.49(1)	121.860(2)	90	125.33(2)
γ, deg	69.046(2)	90	90	90	90
V, Å^3	786.9(2)	1962.8(3)	4027.8(7)	3577(3)	4387.5(12)
Z	2	2	4	4	4
T, K	293(2)	293(2)	293(2)	293(2)	293(2)
ρ (calcd), Mg/m^3	1.162	1.314	1.454	1.339	1.371
μ, mm^{-1}	0.079	0.681	1.369	0.808	1.380
θ range, deg	2.17−27.99	2.25−27.96	1.87−27.98	3.03−27.01	1.89−27.02
no. of rflns/obsd	8456/3418	20820/4345	21494/4578	4459/3902	23449/4764
GOF	1.010	1.008	1.010	1.004	0.861
$R1$	0.0429	0.0372	0.0345	0.0419	0.0424
$wR2$	0.1297	0.0920	0.0857	0.0650	0.0431

[a] $R1 = \Sigma||F_o| - |F_c||/\Sigma|F_o|$, $wR2 = [\Sigma[w(F_o^2 - F_c^2)^2]/\Sigma[w(F_o^2)^2]]^{1/2}$, $w = 1/[\sigma^2(F_o^2) + (aP)^2 + bP]$, where $P = [\max(F_o^2,0) + 2F_c^2]/3$.

Sigma-Aldrich. Synthesis of the LOH ligand was performed under a N_2 atmosphere using standard Schlenk techniques. NMR spectra (^{1}H, ^{13}C, and 2D) were recorded on a Bruker Avance 300 spectrometer. 2D experiments (COSY, NOESY/EXSY, and ^{1}H−^{13}C HSQC) were recorded using standard Bruker pulse sequences. Chemical shifts are reported in ppm referenced to residual solvent protons ($CDCl_3$, CD_3OD, and CD_3OD:D_2O 95:5[14]). Visible spectra were recorded on a Perkin−Elmer Lambda 25 spectrophotometer (range 200−1100 nm) using matched cells of 1 cm path length. Mass spectra were obtained with a Micromass ZMD spectrometer. The mixtures were analyzed in positive-ionization mode by direct perfusion in ESI-MS interface. Infrared spectra were recorded from 4000 to 700 cm^{-1} on a Perkin-Elmer FT−IR Nexus spectrometer equipped with a Thermo-Nicolet microscope. Elemental analyses (C, H, N) were performed with a Carlo Erba EA 1108 automated analyzer.

Synthesis of 4-Methoxy-3,5-dimethyl-2-pyrazol-1-yl-methylpyridine (L).[15] 2-Chloromethyl-4-methoxy-3,5-dimethylpyridine hydrochloride (5.00 g, 22.51 mmol) and pyrazole (1.80 g, 26.44 mmol) were mixed in toluene (150 mL). After adding aqueous NaOH (40% in water, 50 mL) and 30 drops of *n*-tetrabutylammonium hydroxide (40% in water) the mixture was refluxed 4 h with stirring. The organic phase was separated from the aqueous one, washed with water (20 mL), dried with anhydrous Na_2SO_4, and filtered. The solvent was removed under vacuum, and a colorless microcrystalline powder was collected (4.56 g, 93%). IR (cm^{-1}): 3121w, 2966w, 2927w, 1585m, 1569m, 1510s, 1470s, 1438s, 1390s, 1255m, 1089s, 993s, 964s, 874m, 864m, 747vs. ^{1}H NMR (300 MHz, $CDCl_3$): δ 2.25 (s, 6H, CH_3), 3.74 (s, 3H, CH_3O), 5.44 (s, 2H, CH_2), 6.24 (t, J = 2.1 Hz, 1H, C−CH−C pz), 7.43 (d, J = 2.1 Hz, 1H, C−CH−N pz), 7.50 (d, J = 1.4 Hz, 1H, C−CH−N pz), 8.23 (s, 1H, CH py). ^{13}C NMR (75 MHz, $CDCl_3$): δ 11.09 (CH_3), 13.55 (CH_3), 56.24 (CH_3O), 60.13 (CH_2), 106.00 (C−CH−C pz), 126.09 (C quat), 126.44 (C quat), 129.42 (C−CH−N pz), 139.30 (C−CH−N pz), 149.68 (CH py), 164.55 (C quat, C−OCH$_3$). Anal. Calcd for $C_{12}H_{15}N_3O$ (217.27): C, 66.34; H, 6.96; N, 19.34. Found: C, 66.41; H, 7.01; N, 19.18.

(14) Taking as reference δ(CHD_2OD) = 3.34 ppm.
(15) pz = pyrazole, py = pyridine, asterisk (*) = chiral carbon.

Synthesis of 1-(4-Methoxy-3,5-dimethyl-pyridin-2-yl)-2-methyl-1-pyrazol-1-yl-propan-2-ol (LOH). To a THF solution (100 mL) of L (4.56 g, 20.99 mmol) cooled at −78 °C, *n*-BuLi in hexane (1.6 M, 15 mL, 24 mmol) was slowly added. The resulting red solution was stirred for 0.5 h at −78 °C, and then acetone (1.8 mL, 24.51 mmol) was added. The solution was allowed to warm to room temperature, becoming slowly colorless. After 1 h, EtOH 95% (50 mL) was added, and the solution was stirred for 2 h. The cloudy mixture was dried under vacuum, and the solid was extracted with diethyl ether (50 mL). The organic phase was washed with water (3 × 20 mL), dried with anhydrous Na_2SO_4, and filtered. The solvent was removed under vacuum, and a colorless microcrystalline powder was isolated (5.03 g, 87%). Colorless crystals suitable for X-ray diffraction were obtained by stratification of hexane on an ethereal solution of the product. IR (cm^{-1}): 3289m br, 3149w, 2988w, 2975m, 2945w, 1586m, 1567m, 1470s, 1416s, 1396s, 1261s, 1146m, 1086s, 1078s, 1048s, 996s, 801s, 761vs. ^{1}H NMR (300 MHz, CD_3OD): δ 1.02 (s, 3H, CH_3), 1.29 (s, 3H, CH_3), 2.24 (s, 3H, CH_3 py), 2.32 (s, 3H, CH_3 py), 3.79 (s, 3H, CH_3O), 5.61 (s, 1H, CH*), 6.29 (t, J = 2.1 Hz, 1H, C−CH−C pz), 7.50 (d, J = 1.8 Hz, 1H, C−CH-N pz), 7.70 (d, J = 2.4 Hz, 1H, C−CH-N pz), 8.34 (s, 1H, CH py). ^{13}C NMR (75 MHz, CD_3OD): 11.75 (CH_3 py), 14.28 (CH_3 py), 27.99 (CH_3), 29.47 (CH_3), 56.76 (C quat), 61.57 (CH_3O), 68.48 (CH*), 76.19 (C−CH−C pz), 107.63 (C−CH−C pz), 129.36 (C quat), 129.60 (C quat), 131.86 (C−CH−N pz), 139.77 (C−CH−N pz), 149.97 (CH py), 157.89 (C quat), 167.44 (C quat). Anal. Calcd for $C_{15}H_{21}N_3O_2$ (275.35): C, 65.43; H, 7.69; N, 15.26. Found: C, 65.52; H, 7.60; N, 15.24.

Synthesis of [Ni(LOH)$_2$][NiCl$_4$] (1). A solution of LOH (100 mg, 0.36 mmol) in methanol (3 mL) was added dropwise to a methanolic solution (2 mL) of $NiCl_2$·$6H_2O$ (87 mg, 0.37 mmol). The resulting solution was stirred for 15 min. By adding an excess of diethyl ether, a green gluelike precipitate slowly formed. The solvent was removed by suction, and the solid was dissolved in CH_2Cl_2 (5 mL). The mixture was microfiltered and dried under vacuum, yielding a green-light blue powder (102 mg, 0.13 mmol, 72%). IR (cm^{-1}): 3250s br, 3103s br, 2979s, 2866s, 1594m, 1574m, 1470s, 1408s, 1380s, 1294m, 1260s, 1154m, 1115w, 1098w, 1076s, 994m, 845m, 813s, 769s br. ESI-MS (cone 70 V, CH_3OH, *m/z*, I%): 304.4, 100 [Ni(LOH)$_2$]$^{2+}$; 368.3, 10 [Ni(LOH)Cl]$^+$; 607.6, 8

Table 2. Selected Bond Lengths (Å) for **2a**, **3a**, **4a**, and **5a**

2a		**3a**		**4a**		**5a**	
Ni−N(21)	2.051(2)	Cu(1)−N(21)	1.989(2)	Cu−N(21)	1.973(2)	Zn(1)−N(21)	2.098(3)
Ni−N(13)	2.056(2)	Cu(1)−N(13)	2.027(2)	Cu−N(13)	2.033(2)	Zn(1)−N(13)	2.131(2)
Ni−O(12)	2.092(2)	Cu(1)−O(12)	2.331(2)	Cu−O(12)	2.298(2)	Zn(1)−O(12)	2.134(2)
		Cu(2)−Cl(1)	2.242(1)			Zn(2)−Cl(1)	2.227(1)
		Cu(2)−Cl(2)	2.264(1)			Zn(2)−Cl(2)	2.282(1)

Table 3. Logarithms of the Global Formation Constants (β) of the $[M(LOH)]^{2+}$ and $[M(LOH)_2]^{2+}$ Species (M = Ni, Cu, and Zn)[a]

	Ni^{2+}	Cu^{2+}	Zn^{2+}
$\log \beta_1$	2.7(4)	6.4(4)	3.8(1)
$\log \beta_2$	5.3(5)	12.0(5)	7.7(2)
σ[a]	0.02	0.01	0.56

[a] $\sigma^{[a]} = [\Sigma(A_i^\circ - A_i^c)^2/(n-m)]^{1/2}$ = sample standard deviation; A_i° = experimental absorbance or intensity, n = number of observations, and m = number of parameters refined.

$[Ni(LOH)(LO)]^+$. Anal. Calcd for $C_{30}H_{42}N_6O_4Ni_2Cl_4$ (809.88): C, 44.49; H, 5.23; N,10.38. Found: C, 44.53; H, 5.18; N, 10.33.

Synthesis of $[Ni(LOH)_2]Cl_2$ (2). A solution of LOH (100 mg, 0.36 mmol) in methanol (3 mL) was added dropwise to a methanolic solution (2 mL) of $NiCl_2 \cdot 6H_2O$ (43 mg, 0.18 mmol). The resulting violet solution was stirred for 15 min. The product was precipitated with an excess of diethyl ether, filtered, and dried under vacuum, yielding a light violet microcrystalline powder (60 mg, 0.09 mmol, 49%). Crystals suitable for X-ray diffraction were obtained by diffusion of diethyl ether in a methanolic solution of the product, corresponding to $[Ni(LOH)_2]Cl_2 \cdot 3CH_3OH$ (**2a**). IR (cm^{-1}): 3423s, 3381s, 3100s, 2974vs, 2885s, 2777s, 1677w, 1598m, 1574m, 1407s, 1295m, 1216m, 1194w, 1157m, 1082s br, 993 s, 925w, 908w, 886w, 844m, 812s, 778s br. Anal. Calcd for $C_{30}H_{42}N_6O_4NiCl_2$ (680.29): C, 52.97; H, 6.22; N, 12.35. Found: C, 52.89; H, 6.30; N, 12.27.

Synthesis of $[Cu(LOH)_2][CuCl_4]$ (3). A solution of LOH (100 mg, 0.36 mmol) in methanol (3 mL) was added dropwise to a methanolic solution (2 mL) of $CuCl_2 \cdot 2H_2O$ (65 mg, 0.38 mmol). The resulting dark green solution was stirred for 15 min. Dark green crystals of the product (80 mg, 0.10 mmol, 54%), suitable for X-ray diffraction, were obtained by diffusion of diethyl ether in the methanolic solution, corresponding to $[Cu(LOH)_2][CuCl_4] \cdot 2CH_3OH$ (**3a**). IR (cm^{-1}): 3257s br, 3098s, 2973s, 1596s, 1572m, 1472s br, 1409s, 1294s, 1264vs, 1159s, 1078vs, 989s, 920w, 811s, 773s. ESI-MS (cone 70 V, CH_3OH, *m/z*, I%): 306.8, 25 $[Cu(LOH)_2]^{2+}$; 338.4, 10 $[Cu(LO)]^+$; 370.4, 20 $[Cu(LOH)(CH_3OH)]^+$; 612.5, 2 $[Cu(LOH)(LO)]^+$. Anal. Calcd for $C_{30}H_{42}N_6O_4Cu_2Cl_4$ (819.59): C, 43.96; H, 5.16; N, 10.25. Found: C, 44.05; H, 5.21; N, 10.15.

Synthesis of $[Cu(LOH)_2]Cl_2$ (4). A solution of LOH (100 mg, 0.36 mmol) in methanol (3 mL) was added dropwise to a methanolic solution (2 mL) of $CuCl_2 \cdot 2H_2O$ (31 mg, 0.18 mmol). The resulting bright blue solution was stirred for 15 min. Blue crystals of the product (87 mg, 0.13 mmol, 70%), suitable for X-ray diffraction, were obtained by diffusion of diethyl ether in the methanolic solution, corresponding to $[Cu(LOH)_2]Cl_2 \cdot 2H_2O$ (**4a**). IR (cm^{-1}): 3476s, 3406s, 3104s br, 2977m, 2739w, 2527w, 1624w, 1595m, 1407s, 1380s, 1296m, 1260vs, 1188w, 1156s, 1076vs, 993s, 846m, 812s, 766vs. Anal. Calcd for $C_{30}H_{42}N_6O_4CuCl_2$ (685.14): C, 52.59; H, 6.18; N, 12.27. Found: C, 52.63; H, 6.22; N, 12.19.

Synthesis of $[Zn(LOH)_2][ZnCl_4]$ (5). A solution of LOH (100 mg, 0.36 mmol) in methanol (3 mL) was added dropwise to a methanolic solution (2 mL) of $ZnCl_2$ (50 mg, 0.37 mmol). The resulting colorless solution was stirred for 15 min. The product was precipitated with an excess of diethyl ether, filtered, and dried under vacuum, yielding a colorless microcrystalline powder (128 mg, 0.31 mmol, 86%). Crystals suitable for X-ray diffraction were obtained by diffusion of diethyl ether in an acetonitrile solution of the product, corresponding to $[Zn(LOH)_2][ZnCl_4] \cdot 2CH_3CN$ (**5a**). IR (cm^{-1}): ~3430br, ~3230br, 3103s, 2936s, 2974s, 1593m, 1570m, 1512w, 1406s, 1289m, 1187w, 1150m, 1073s br, 990m, 954w, 922w, 809m, 769m. ^1H NMR spectrum (300 MHz, $CD_3OD:D_2O$ 95:5): see discussion for Zn^{2+}:LOH 1:1 ratio. ESI-MS (cone 25 V, CH_3OH, *m/z*, I%): 307.3, 100 $[Zn(LOH)_2]^{2+}$; 374.0, 10 $[Zn(LOH)Cl]^+$; 613.2, 20 $[Zn(LOH)(LO)]^+$. Anal. Calcd for $C_{30}H_{42}N_6O_4ZnCl_2$ (823.28): C, 43.77; H, 5.14; N, 10.21. Found: C, 43.70; H, 5.20; N, 10.29.

X-ray Crystallography. A summary of data collection and structure refinement for the ligand LOH and compounds $[Ni(LOH)_2]Cl_2 \cdot 3CH_3OH$ (**2a**), $[Cu(LOH)_2][CuCl_4] \cdot 2CH_3OH$ (**3a**), $[Cu(LOH)_2]Cl_2 \cdot 2H_2O$ (**4a**), and $[Zn(LOH)_2][ZnCl_4] \cdot 2CH_3CN$ (**5a**) is reported in Table 1. Single-crystal data was collected with a Bruker AXS Smart 1000 area detector diffractometer (Mo Kα: $\lambda = 0.71073$ Å, LOH, **2a**, **3a**, and **5a**) and a Philips PW 1100 diffractometer (Mo Kα: $\lambda = 0.71073$ Å, **4a**). Cell parameters were refined from the observed setting angles and detector positions of selected strong reflections for LOH, **2a**, **3a**, and **5a**. Intensities were integrated from several series of exposures frames covering the sphere of reciprocal space.[16] For **4a** the cell constants were obtained by a least-square refinement of the setting angles of 24 randomly distributed and carefully centered reflections. An absorption correction was applied using the program SADABS[17] with transmission factors in the ranges 0.830−1.000 (LOH), 0.715−1.000 (**2a**), 0.794−1.000 (**3a**), and 0.752−1.000 (**5a**) and using the method of Walker and Stuart[18] for **4a** with min and max transmission factors of 0.886 and 1.000. The structures were solved by direct methods (SIR97[19]) and refined on F^2 with full-matrix least squares (SHELXL-97[20]), using the Wingx software package.[21] Non-hydrogen atoms were refined anisotropically for all compounds. The hydrogen atom of the hydroxyl group was found and refined for all compounds, whereas the remaining hydrogen atoms of the ligands were placed at their calculated positions. One of the three solvent molecules of crystallization (CH_3OH) in **2a** was found disordered in two positions with a site occupancy factor of 0.5 for each molecule. For **3a**, the independent crystallization solvent molecule was found disordered in three positions, each with a site occupancy factor of 0.33. Graphical material was prepared with ORTEP3 for Windows.[22]

(16) *SMART (control) and SAINT (integration) software for CCD systems*; Bruker AXS: Madison, WI, 1994.
(17) *Area-Detector Absorption Correction*; Siemens Industrial Automation, Inc.: Madison, WI, 1996.
(18) Walker, N.; Stuart, D. *Acta. Crystallogr.* **1983**, *A39*, 158−166.
(19) Altomare, A.; Burla, M. C.; Camalli, M.; Cascarano, G. L.; Giacovazzo, C.; Guagliardi, A.; Moliterni, A. G. G.; Polidori, G.; Spagna, R. *J. Appl. Crystallogr.* **1999**, *32*, 115.
(20) Sheldrick, G. M. *SHELX97. Programs for Crystal Structure Analysis*, Release 97-2; University of Göttingen: Göttingen, Germany, 1997.
(21) Farrugia, L. J. J. *Appl. Crystallogr.* **1999**, *32*, 837.
(22) Farrugia, L. J. J. *Appl. Crystallogr.* **1997**, *30*, 565.

Table 4. Relaxation Matrix Containing the Exchange Constants k^{ex}_{ij} (i = column, j = row, s^{-1}) between the Different Zn^{2+}/LOH Species in CD_3OD (1A, 2A−E, see Figure 9)[a]

	X	**Y_1**	**Z_1**	**Z_2**	**Y_2**	**Z_3**	**Y_3**
X	[Zn(LOH)$_2$]$^+$ → [Zn(LOH)Cl]$^+$ ⇨ / [Zn(LOH)Cl]$^+$ → [Zn(LOH)$_2$]$^+$ ⇩	0.03(1)	0.07(1)	0.05(1)	0.05(2)	0.06(1)	0.07(2)
Y_1	0.06(2)		-	-	0.48(4)	-	0.14(7)
Z_1	0.13(3)	-		1.8(1)	-	1.7(2)	-
Z_2	0.09(2)	-	1.4(1)		-	0.12(9)	-
Y_2	0.12(3)	0.45(2)	-	-		-	2.7(3)
Z_3	0.12(2)	-	1.3(2)	0.11(8)	-		-
Y_3	0.15(5)	0.13(6)	-	-	2.6(3)	-	⇖ [Zn(LOH)$_2$]$^+$ → ([Zn(LOH)$_2$]$^+$)$^\#$

[a] The corresponding X, Y_{1-3}, and Z_{1-3} exchanging sites (NMR Signals) are reported in the same order of the EXSY spectrum (see Figure 8).

DFT Calculations. All calculations were performed with Gaussian 03 software.[23] Assuming that the ligand LOH is a racemic mixture of the *R* and *S* enantiomers, five possible octahedral $[Zn(LOH)_2]^{2+}$ complexes can be obtained: three *RR*/*SS* enantiomeric pairs, the *RS*/*SR* noncentrosymmetric pair, and the *RS* centrosymmetric complex (see discussion). For optimization of the molecular geometry of the five $[Zn(LOH)_2]^{2+}$ model complexes, in which the methyl groups were replaced by hydrogen atoms, the gradient-corrected hybrid density functional B3LYP[24,25] and the 6-31+G basis set were used. Single-point energy calculations were performed using the B3LYP density functional and the 6-311+G(d) basis set. The energies of the various compounds do not include thermal or entropy corrections.

Visible and NMR Titrations. Complexation of M^{2+} ions (M = Ni, Cu, Zn) with the ligand LOH was studied in a methanol: water 95:5 (v/v) mixture at T = 25 °C by spectrophotometric titrations in the visible range (400−900 nm). Ni^{2+} and Cu^{2+} stock solutions (C_{Ni} = 0.207 M; C_{Cu} = 0.035 M) were prepared by weight from their chloride salts and contained NMe_4Cl as an ionic medium (C_{NMe4Cl} = 0.46 M). Metal ions and ligand stock solutions (prepared by weight) were used immediately. Speciation of the Ni^{2+} or Cu^{2+}/LOH systems was studied by collecting visible spectra of batch samples containing a fixed metal-ion concentration with increasing concentrations of ligand up to 1:2.71 (Ni^{2+}/LOH) and 1:2.26 (Cu^{2+}/LOH) ratios. Speciation of the Zn^{2+}/LOH system was investigated by collecting ^{1}H NMR spectra[26] of a 0.009 M ligand sample titrated with aliquots of a 0.05 M $ZnCl_2$ solution (up to a 7.4:1 Zn^{2+}:LOH ratio). Visible spectrophotometric data were treated by means of the SPECFIT32 program,[26] which allowed determination of both the complexation log β values and the molar absorbancies of the complex species. For the Zn^{2+}/LOH system, the equilibria between LOH, $[Zn(LOH)Cl]^+$, and $[Zn(LOH)_2]^{2+}$ occur in the slow-exchange NMR condition, with the inconvenience of signal overlap between various species. Nevertheless, the observed intensity at a certain chemical shift can be expressed by the sum of the integrals appearing at that chemical shift value if all the contributions derive from the same type of protons. This is expressed by

$$I_\delta^* = \sum_{\text{species},\delta} {I_L}^{0*}\chi_\delta^{\text{species}} nm = \sum_{\text{species},\delta} \frac{{I_L}^{0*}}{C_L} nm C_\delta^{\text{species}}$$

(23) Frisch, M. J.; Trucks, G. W.; Schlegel, H. B.; Scuseria, G. E.; Robb, M. A.; Cheeseman, J. R.; Montgomery, J. A., Jr.; Vreven, T.; Kudin, K. N.; Burant, J. C.; Millam, J. M.; Iyengar, S. S.; Tomasi, J.; Barone, V.; Mennucci, B.; Cossi, M.; Scalmani, G.; Rega, N.; Petersson, G. A.; Nakatsuji, H.; Hada, M.; Ehara, M.; Toyota, K.; Fukuda, R.; Hasegawa, J.; Ishida, M.; Nakajima, T.; Honda, Y.; Kitao, O.; Nakai, H.; Klene, M.; Li, X.; Knox, J. E.; Hratchian, H. P.; Cross, J. B.; Bakken, V.; Adamo, C.; Jaramillo, J.; Gomperts, R.; Stratmann, R. E.; Yazyev, O.; Austin, A. J.; Cammi, R.; Pomelli, C.; Ochterski, J. W.; Ayala, P. Y.; Morokuma, K.; Voth, G. A.; Salvador, P.; Dannenberg, J. J.; Zakrzewski, V. G.; Dapprich, S.; Daniels, A. D.; Strain, M. C.; Farkas, O.; Malick, D. K.; Rabuck, A. D.; Raghavachari, K.; Foresman, J. B.; Ortiz, J. V.; Cui, Q.; Baboul, A. G.; Clifford, S.; Cioslowski, J.; Stefanov, B. B.; Liu, G.; Liashenko, A.; Piskorz, P.; Komaromi, I.; Martin, R. L.; Fox, D. J.; Keith, T.; Al-Laham, M. A.; Peng, C. Y.; Nanayakkara, A.; Challacombe, M.; Gill, P. M. W.; Johnson, B.; Chen, W.; Wong, M. W.; Gonzalez, C.; Pople, J. A. *Gaussian 03*, Revision C.02; Gaussian, Inc.: Wallingford, CT, 2004.

(24) Becke, A. D. *Phys. Rev. A* **1988**, *38*, 3098−3100.

(25) Becke, A. D. *J. Chem. Phys.* **1993**, *98*, 5648−5652.

(26) (a) Binstead, R. A.; Jung, B.; Zuberbühler, A. D. *Specfit/32*, Ver.3.0; Spectrum Software Associates: Marlborough, MA. (b) Gampp, H.; Maeder, M.; Meyer, C. J.; Zuberbühler, A. D. *Talanta* **1985**, *32*, 256−264.

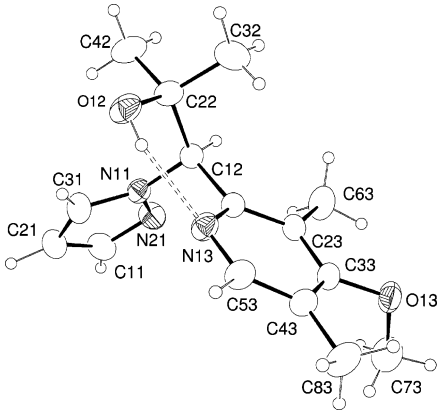

Figure 1. ORTEP drawing of the ligand LOH at the 30% thermal ellipsoids probability level. Selected bond distances (Å): O(12)−C(22) = 1.425(2), N(13)−C(53) = 1.337(2), N(13)−C(13) = 1.339(2), N(21)−C(11) = 1.326-(2), N(21)−N(11) = 1.354(2).

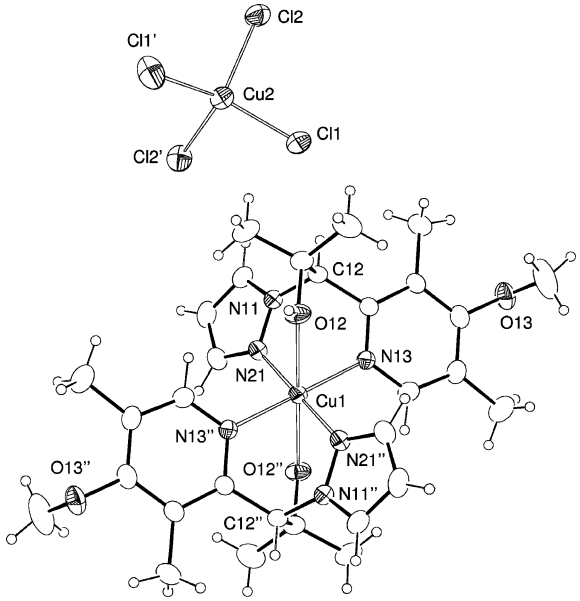

Figure 2. ORTEP drawing of $[Cu(LOH)_2][CuCl_4]$·2MeOH (**3a**) at the 30% thermal ellipsoids probability level. The CH_3OH solvent molecules were omitted for clarity. Single prime (′) = $-x$, y, $1/2 - z$; double prime (″) = $1/2 - x$, $1/2 - y$, $-z$.

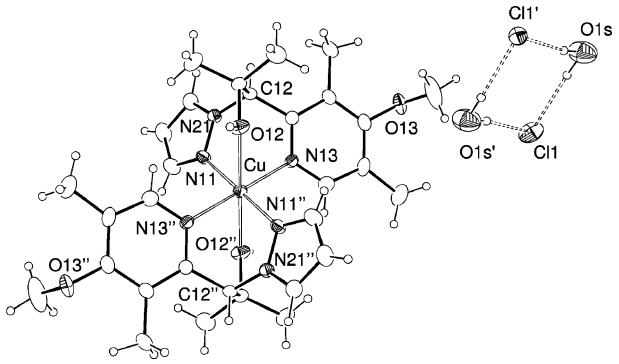

Figure 3. ORTEP drawing of $[Cu(LOH)_2]Cl_2$·$2H_2O$ (**4a**) at the 30% thermal ellipsoids probability level. Single prime (′) = $-x$, $1 - y$, $1 - z$; double prime (″) = $-x$, $-y$, $-z$.

where I_δ* = observed integral at chemical shift δ, $I_L{}^{0}$* = ligand one-proton integral at the initial condition, χ_d = mole fraction of the species (LOH, $[M(LOH)Cl]^+$, or $[M(LOH)_2]^{2+}$) with protons absorbing at chemical shift δ, n = number of protons of the

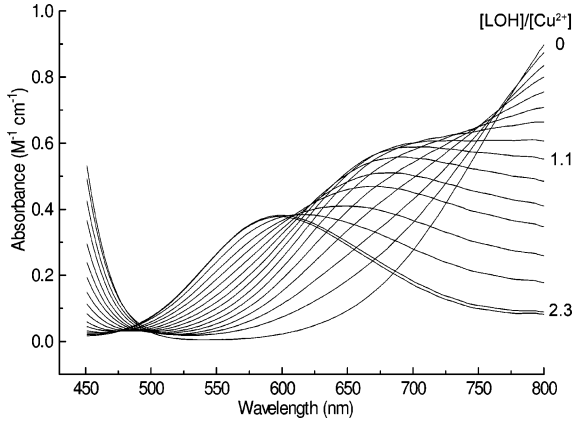

Figure 4. Experimental visible spectra for the spectrophotometric titration of $CuCl_2$·$2H_2O$ with LOH (Cu^{2+}:LOH = 1:0−2.26, C_{Cu} = 0.018 M).

Scheme 4

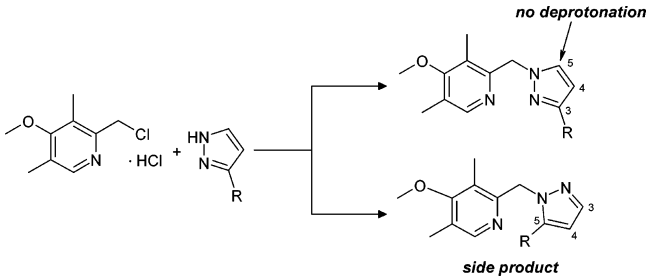

functional groups at chemical shift δ of each species, m = number of ligands in the absorbent species, C_L = total ligand concentration. I_δ* and $I_L{}^{0}$* were normalized for the internal standard integral (TMS). The right side of eq 1 closely resembles the Lambert−Beer equation for an optical path length of 1 cm and $\epsilon = (nmI_L{}^{0}*/C_L)$. On this ground, least-square regression calculation procedures, employed to treat UV−vis spectroscopic data, can be applied to the treatment of slow-exchange NMR data. In this work, the SPECFIT32 program was used for the calculations. Application of this pseudo-Lambert−Beer equation to obtain global formation constants (β) simply consists of introduction of the $nmI_L{}^{0}*/C_L$ values (pseudo-ϵ) for each of the signals taken into account in the calculations together with the I_δ* (pseudo-adsorbance). Species which do not possess protons absorbing at a given chemical shift δ are treated with $nmI_L{}^{0}*/C_L = 0$.

EXSY Spectroscopy. $^1H-^1H$ EXSY spectra of **5** were recorded in CD_3OD at 300 K using a conventional phase-sensitive NOESY pulse sequence employing different mixing times (τ_m): 0.2, 0.4, 0.6, and 0.8 s. The method of Perrin was applied to calculate the exchange rate constants:[27] $\mathbf{R} = \ln \mathbf{A}/\tau_m$, where **R** is the relaxation matrix, which contains exchange constants $k_{ij}{}^{ex}$ (i = starting species/proton, j = derived species/proton) as diagonal elements and **A** is a matrix whose elements are $I_{ij}(\tau_m)/M_j{}^{0}$ (I_{ij} = volumes of the 2D peaks, $M_j{}^{0}$ = volumes of the diagonal peaks at $\tau_m = 0$). The final $k_{ij}{}^{ex}$ elements are reported as the mean value of the experimental $k_{ij}{}^{ex}$ (τ_m) obtained at different mixing times, Table 4.[28] Rate constants k_{ij} and semi-reaction rates r_{ij} were calculated from $k_{ij}{}^{ex}$ by considering a first-order mechanism for interconversion of the $[Zn(LOH)_2]^{2+}$ isomers and a second-order one for exchange between $[Zn(LOH)Cl]^+$ and the octahedral $[Zn(LOH)_2]^{2+}$ species (see Supporting Information). Equilibrium concentrations were derived from integration of the diagonal peak volumes at $\tau_m = 0$

(27) Perrin, C. L.; Dwyer, T. J. *Chem. Rev.* **1990**, *90*, 935−967.
(28) *EXSY-Calculator program*; MestreLab Research: www.mestrec.com.

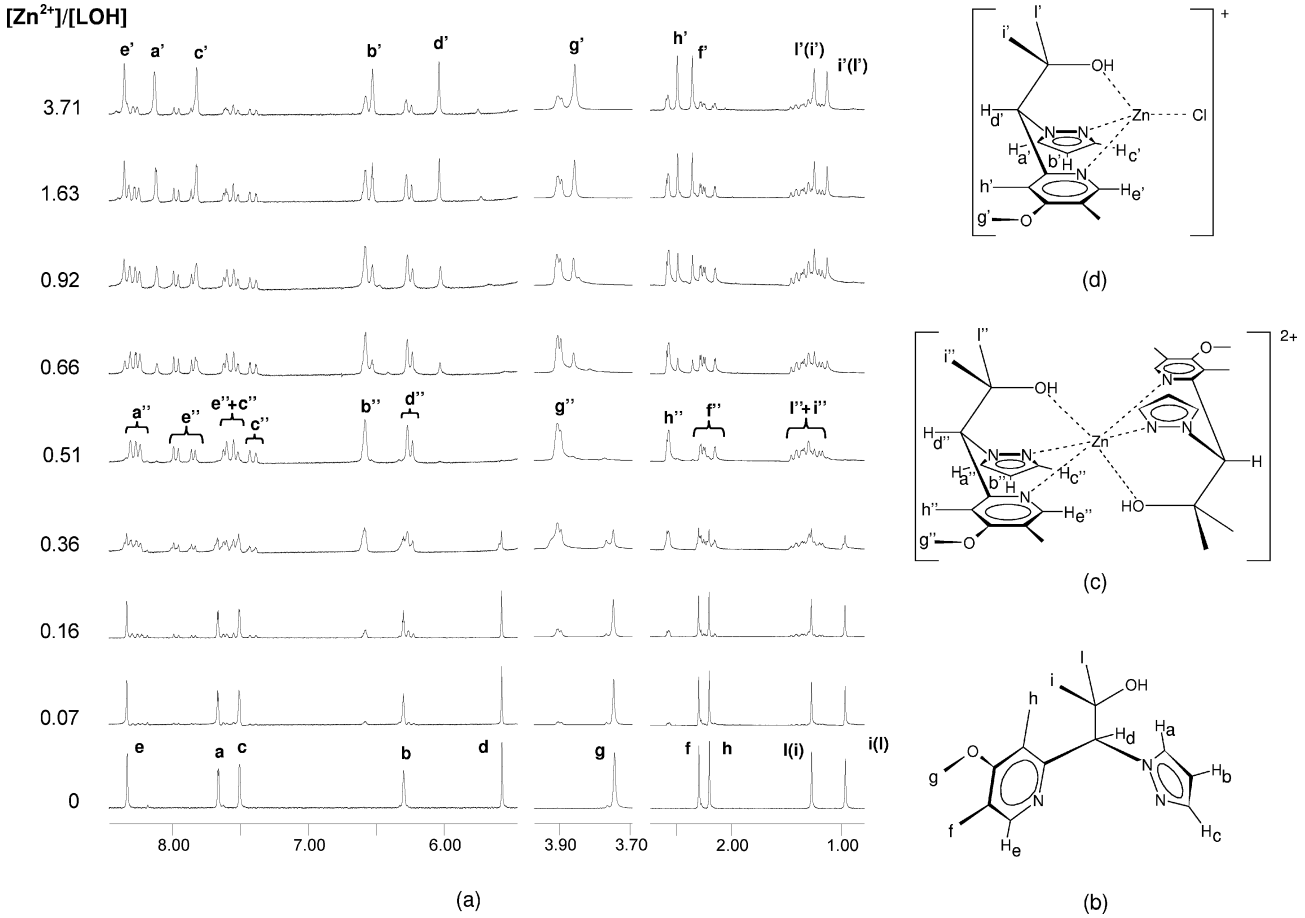

Figure 5. ^{1}H NMR titration of the Zn^{2+}/LOH system (a). The assignment of the different NMR signals for each Zn^{2+}/LOH species is reported in (b), (c), and (d) for LOH, $[Zn(LOH)Cl]^+$, and $[Zn(LOH)_2]^{2+}$, respectively.

and from the analytical concentration of Zn in the solution (C_{Zn} = 0.015 M). Uncertainties of k_{ij} and of r_{ij} were calculated by propagation and neglecting concentration errors.

3. Results and Discussion

The two-step LOH synthesis is described in Scheme 3. The first reaction between the electrophilic chloromethyl−dimethylpyridine derivative and pyrazole, performed in biphasic solvent (toluene/water) via phase-transfer catalysis (*n*-Bu_4NOH), is analogous to a procedure reported in the literature.[29] The second step involves insertion of an electrophile on the generated carbanion in agreement with the method developed for the synthesis of bis(pyrazolyl)methane derivatives.[2a] Use of acetone as an electrophile provides the N,N′,O-heteroscorpionate ligand LOH in good yield. Selective deprotonation of the methylene bridge without competition from other acidic groups, such as the C5 proton on pyrazole,[30] is favored by the benzylic-like character of the conjugated base. Moreover, the methyl substituents on pyridine allow electrophile insertion exclusively on the bridging carbon and not on the 3 and 5 positions of the pyridine ring. This synthetic pathway has a more general application concerning the preparation of mixed N,N′,X (X = heteroatom) scorpionates. In fact, variously substituted pyrazoles can be, in principle, employed without the drawbacks of pyrazole deprotonation on the C5 position. However, it has to be noted that when a monosubstituted pyrazole is employed, two structural isomers can be obtained depending on which pyrazole nitrogen atom is eventually attached to the bridging methylene group, Scheme 4. Nevertheless, this inconvenience has minimum consequences since the reaction usually favors the isomer which is unsubstituted on the C5-pyrazole position (unpublished data). Furthermore, the stability of the pyrazole−pyridine conjugate base (with respect to the bispyrazolyl one) allows it to react with electrophiles that exhibit weak acidic character such as acetone. LOH is a chiral molecule due to the asymmetry of the bridging carbon atom, although it was obtained in a racemic mixture. On the other hand, introduction of a stereogenic center on analogous bis(pyrazolyl)methane derivatives requires use of two differently substituted pyrazoles, a procedure that can generate at least three possible products (two symmetric compounds and the prochiral molecule) with subsequent low yields and purification/separation inconveniences.[12] We did not perform the chiral resolution of LOH, and it is worth considering that the acidic nature of the bridging CH may limit the use of the ligand in its *R* or *S*

(29) House, D. A.; Steel, P. J.; Watson, A. A. *Aust. J. Chem.* **1986**, *39*, 1525−1536.

(30) (a) Katritzky, A. R.; Abdel-Rahman, A. E.; Leahy, D. E.; Schwarz, O. A. *Tetrahedron* **1983**, *39*, 4133−4142. (b) Antiñolo, A.; Carrillo-Hermosilla, F.; Díez-Barra, E.; Fernández-Baeza, J.; Fernández-López, M.; Lara-Sánchez, A.; Moreno, A.; Otero, A.; Rodríguez, A. M. *Dalton Trans.* **1998**, 3737−3743.

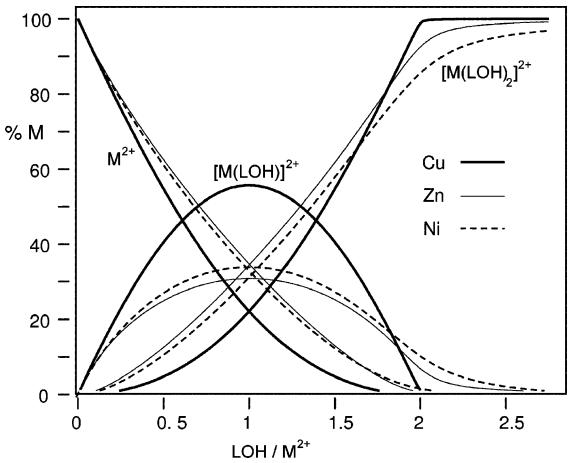

Figure 6. Distribution diagram of the M^{2+}/LOH systems (M = Ni, Cu, Zn).

enantiopure forms since in the presence of mild basic conditions they may be subject to racemization.

The donor ability of the neutral LOH ligand versus 3d late transition metal ions was investigated by reacting LOH with MCl_2 salts (M^{2+} = Ni^{2+}, Cu^{2+}, and Zn^{2+}) in both 1:1 and 1:2 M^{2+}:LOH ratios that exclusively gave $[M(LOH)_2]^{2+}$ cationic complexes. For Ni^{2+} and Cu^{2+}, the M^{2+}:LOH stoichiometric ratio determined the type of counterions, which was Cl^- or $[MCl_4]^{2-}$ for M^{2+}:LOH of 1:2 and 1:1, respectively, whereas for Zn^{2+} only the complex $[Zn(LOH)_2][ZnCl_4]$ was isolated, regardless of stoichiometric conditions. We attempted to explore the coordination properties of the deprotonated ligand LO^- with Zn^{2+} in a 1:1 ratio in order to obtain a [Zn(LO)Cl] neutral complex in analogy to bis-(pyrazolyl)-alkoxides.[3f,7a,b] The Li(LO) alkoxide was prepared by deprotonating the alcoholic function of LOH using *n*-BuLi in THF. The reaction with anhydrous $ZnCl_2$ did not give the desired [Zn(LO)Cl] complex since decomposition of LOH occurred, presumably in a metal-catalyzed pathway, which generated the ligand precursor L^- and acetone, followed by protonation of L^- by adventitious moisture. In fact, the $[Zn(L)Cl_2]$ complex was isolated from this reaction and structurally characterized. This complex could also be prepared by direct reaction between $ZnCl_2$ and L in methanol (Supporting Information).

Solid-State Structures. The molecular structures of the ligand LOH and of the complexes $[Cu(LOH)_2][CuCl_4]\cdot 2CH_3OH$ (**3a**) and $[Cu(LOH)_2]Cl_2\cdot 2H_2O$ (**4a**) are reported in Figures 1−3, while the molecular geometry of the $[Ni(LOH)_2]Cl_2\cdot 3CH_3OH$ (**2a**) and $[Zn(LOH)_2][ZnCl_4]\cdot 2CH_3CN$ (**5a**) complexes is reported in the Supporting Information. Selected geometric parameters are listed in Table 2. The main difference between the free and coordinated LOH resides in the different orientation of the pyrazole and pyridine groups with respect to the central C atom since in the free ligand they point in opposite directions in order to minimize the N lone-pair repulsion. In addition, in the free ligand the hydroxyl group acts as hydrogen-bond donor with the pyridine nitrogen atom (d[O(12)−N(13)] = 2.741(2) Å). In **3a** and **4a** the metal lies on a crystallographic inversion center and the complexes present a distorted octahedral geometry

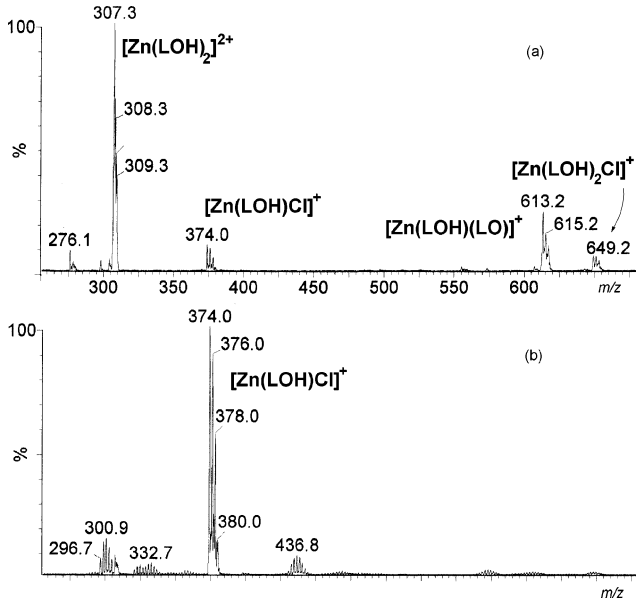

Figure 7. ESI-MS spectra of the Zn^{2+}/LOH system in a 1:1 (a) and ∼10:1 (b) ratio in methanol.

with the equatorial plane defined by the nitrogen atoms of two pyrazole and two pyridine groups from two N,N′,O-chelate ligands. The apical positions are occupied by two hydroxyl groups, and the Cu−O bond lengths are ≈0.3 Å greater than the Cu−N one (d[Cu−O(12)] is 2.331(2) Å for **3a** and 2.298(2) Å for **4a**), as a consequence of the tetragonal distortion typical of the Cu^{2+} ion. The $[CuCl_4]^{2-}$ counteranion of **3a** adopts a geometry intermediate between the square planar and the tetrahedral one. The tetrahedron is flattened along the Cl(1)−Cu(1)−Cl(1)′ (141.30(6)°) and Cl(2)−Cu(1)−Cl(2)′ (140.53(5)°, single prime (′) = $-x$, y, 1/2 − z) angles bisector. The chlorine anions of **4a** are exchanging hydrogen bonds with two crystallization water molecules. In addition, the hydroxyl groups of **3a** and **4a** behave as hydrogen-bond donors with the Cl(2) chlorine anion (d[O(12)−Cl(2)″] = 3.216(2) Å, double prime (″) = 1 − x, y − 1, 1/2 − z) and with the Cl(1) chlorine anion (d[O(12)−Cl(1)‴] = 3.063(3) Å, triple prime (‴) = 1/2 + x, 1/2 − y, $-z$), respectively.

The molecular structures of the Zn^{2+} and Ni^{2+} complexes are in agreement with the structure reported for compounds **3a** and **4a**. The metal, in both complexes, lies on an inversion center and is in a regular octahedral geometry with M-(donor atom) bond distances that essentially reflect the differences between the ionic radii of the two metals (range distances: Ni^{2+}−donor = 2.051(2)−2.092(2) Å, Zn^{2+}−donor = 2.098(3)−2.134(2) Å), Table 2. The $[ZnCl_4]^{2-}$ counterion of **5a** exhibits a regular tetrahedral geometry with Cl−Zn−Cl angles in the range 105.70(5)−116.10(5)°. It is worth noting that LOH is forced to behave as tridentate N,N′,O by the presence of the methyl groups of the tertiary OH group. In fact, rotation along the C(12)−C(22) bond would displace the OH from coordination but bring one of the methyl groups in close proximity to the metal.

Solution Studies. Speciation of the three M^{2+}/LOH systems (M^{2+} = Ni^{2+}, Cu^{2+}, Zn^{2+}) was evaluated in a methanol:water 95:5 solution by titration methods. The

Scheme 5

$$M^{2+} + LOH \overset{\beta_1}{\rightleftharpoons} [M(LOH)]^{2+}$$

$$M^{2+} + 2LOH \overset{\beta_2}{\rightleftharpoons} [M(LOH)_2]^{2+}$$

choice of the solvent depends on the solubility properties of both the MCl_2 salts and the ligand, Figures 4 and 5. For all of the M^{2+}/LOH systems, three-species equilibria were obtained (Scheme 5), and the distribution diagrams are reported in Figure 6. The global formation constants (β) of the $[M(LOH)]^{2+}$ and $[M(LOH)_2]^{2+}$ complexes are in agreement with the Irving−Williams series ($Ni^{2+} < Cu^{2+} > Zn^{2+}$), Table 3.[31] Cu^{2+} complexation constants with LOH are close to those determined for the bidentate di-2-pyridylmethane, despite the fact that LOH is coordinated to copper in a tridentate fashion. Actually, the formation constants in aqueous solution of the Cu^{2+}/di-2-pyridylmethane complexes are log $\beta_{[ML]} = 6.7$ and log $\beta_{[ML2]} = 11.8$ ($T = 20$ °C, $I = 0.1$ M).[32] Compared to this ligand, LOH possesses a third coordinating site (−OH) and a pyrazole moiety in place of the pyridyl group. It is known that *N*-methyl-3,4-dimethylpyrazole complexes with Cu^{2+} are less stable that those of pyridine (i.e., log $\beta_1 = 1.6$ and 2.54, respectively). It is then reasonable that the lower stability imparted by the pyrazole if compared to a pyridyl residue and the presence of the additional OH group in LOH in a sterically favorable position compensate for each other. In addition, LOH gives greater stability constants with Zn^{2+} than with Ni^{2+}, different than for the above-mentioned di-2-pyridylmethane, which gives greater complexation constants with Ni^{2+} (log $\beta_{[ML]} = 5.02$) than with Zn^{2+} (log $\beta_{[ML]} = 2.81$). In LOH, the presence of the OH group may increase the *hard* character of the ligand, in favor of the Zn^{2+} complexes stability. Metal coordination of the $[M(LOH)]^{2+}$ species is most probably completed by chlorine ions or solvent molecules, whereas it is easy to describe the $[M(LOH)_2]^{2+}$ complexes as octahedral, analogous with the X-ray structures. In fact, the hypothesis of pentacoordinate $[M(LOH)_2]^{2+}$ species is excluded for steric reasons since the OH group is forced to be coordinated when the pyridine and pyrazole nitrogen atoms are bound to the metal (see section 3.2). ESI-MS spectra recorded from a methanolic solution of **1**, **3**, and **5** (M:LOH = 1:1) revealed the occurrence of the $[M(LOH)_2]^{2+}$ complex together with the $[M(LOH)Cl]^+$ (Ni^{2+} and Zn^{2+}) and $[Cu(LOH)(CH_3OH)]^+$ species. In addition, in the ESI-MS spectrum obtained from a solution of **5** containing a large excess of Zn^{2+} (Zn^{2+}:LOH 10:1), only the peak of the $[Zn(LOH)Cl]^+$ complex was present, Figure 7. This would provide evidence for the chlorine and solvent coordination to the $[M(LOH)]^{2+}$ moiety but also support the molecular structures reported in Figure 5, with the $[Zn(LOH)Cl]^+$ complex exhibiting a tetrahedral structure bound by the N,N′,O ligand and by an apical chlorine ion. The $[M(LOH)_2]^{2+}$ ($M^{2+} = Cu^{2+}$ and Zn^{2+}) complexes crystallized also in 1:1 M^{2+}:LOH stoichiometric conditions were probably due to formation of a stable ion pair between $[M(LOH)_2]^{2+}$ and $[MCl_4]^{2-}$. Another reason for this can be derived from the analysis of the distribution diagram reported in Figure 6, where it is evident that with a 1:1 M^{2+}:LOH ratio the global $[MCl_4]^{2-}+[M(LOH)_2]^{2+}$ concentration is greater than or comparable to the $[M(LOH)]^{2+}$ species concentration. Moreover, $[Zn(LOH)_2][ZnCl_4]$ is precipitated from a solution containing a 1:2 Zn^{2+}:LOH ratio. This probably occurs as a consequence of favorable packing forces between the tetrahedral $[ZnCl_4]^{2-}$ and octahedral $[Zn(LOH)_2]^{2+}$.

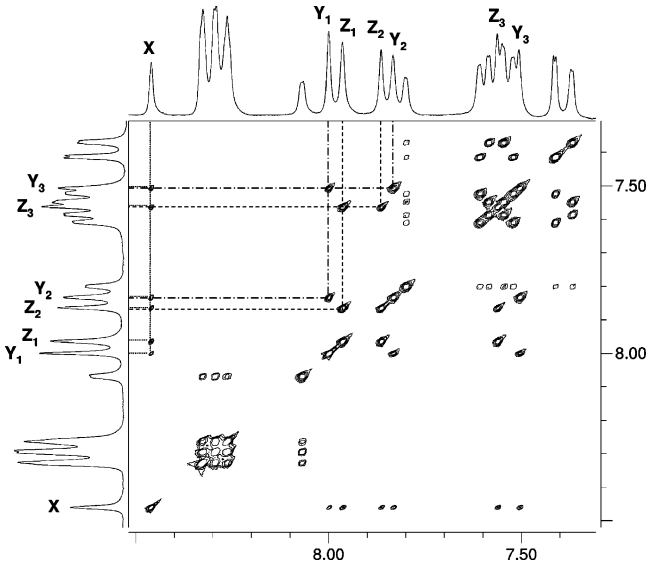

Figure 8. $^1H-^1H$ EXSY spectrum of **5** in CD_3OD registered at 300 K in the 7.25−8.55 ppm range (mixing time = 0.8 s). The pyridyl protons of $[Zn(LOH)Cl]^+$ (X) and the $[Zn(LOH)_2]^{2+}$ isomers (Y_{1-3} and Z_{1-3}) are evidenced. Exchange between X and the two groups of Y_{1-3} and Z_{1-3} protons (····); exchange within the two groups of Y_{1-3} and Z_{1-3} protons (− ■ − and − − −).

In Figure 5 the ^1H NMR titration in CD_3OD:D_2O 95:5 of the Zn^{2+}/LOH system together with the signal assignment of LOH, $[Zn(LOH)Cl]^+$, and $[Zn(LOH)_2]^{2+}$ is reported. In the presence of the maximum concentration of $[Zn(LOH)_2]^{2+}$ (for a 0.5 Zn^{2+}:LOH ratio), various sets of signals appear in the ^1H NMR spectrum, whereas when increasing the Zn^{2+} concentration (up to ≈4 fold with respect to LOH) only a set of signal appears. This is in agreement with the ESI-MS findings, suggesting that the $[Zn(LOH)Cl]^+$ complex becomes preponderant when increasing the Zn^{2+} concentration. It is helpful to resort to 2D NMR techniques for elucidation of the equilibria occurring between the various solution species. The $^1H-^1H$ NOESY/EXSY spectrum of **5** registered at 300 K ($\tau_m = 0.6$ s), along with the negative cross-peaks deriving from cross-relaxation (NOE), shows a set of positive cross-peaks (same diagonal sign) disappearing at 250 K ($\tau_m = 0.6$ s), which are due to chemical exchange between different species in solution (Supporting Information). In order to quantitatively analyze the chemical exchange processes, a series of more resolved EXSY spectra were registered in the 7.25−8.55 ppm range and at various τ_m (0.2, 0.4, 0.6, 0.8 s) that focused on the set of seven well-separated pyridyl protons (Figure 8). According to the NMR titration, the X proton belongs to the $[Zn(LOH)Cl]^+$ tetrahedral species (1A, Figure 9), while the other six (Y_1, Y_2,

(31) (a) Irving, H.; Williams, R. J. P. *J. Chem. Soc.* **1953**, 3192−3210. (b) Sigel, H.; McCormick, D. B. *Acc. Chem. Res.* **1970**, *3*, 201−208.
(32) Martell, A. E.; Smith, R. M. *NIST Standard Reference Database 46*, Version 7.0; NIST: Gaithersburg, MD, 2003.

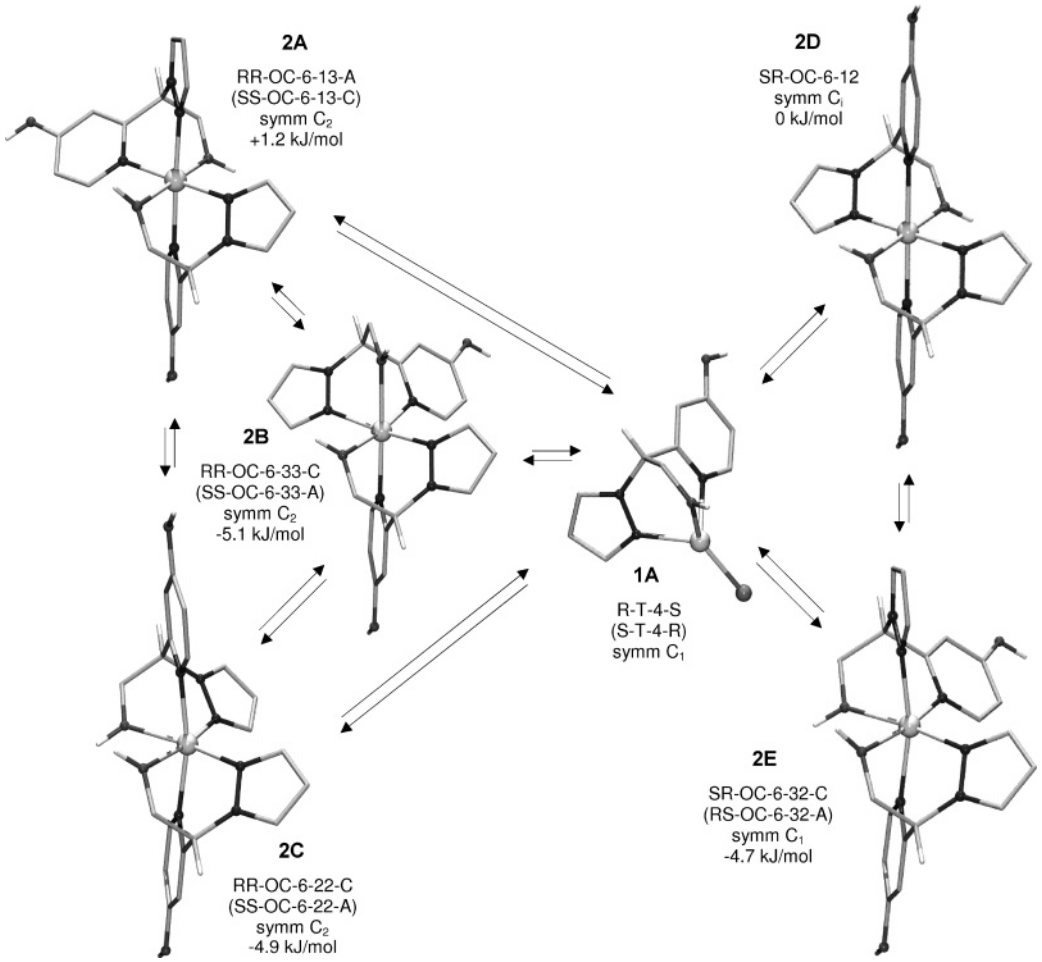

Figure 9. DFT-optimized model complexes of the $[Zn(LOH)_2]^{2+}$ (2A−E) and $[Zn(LOH)Cl]^{+}$ (1A) species together with the equilibrium scheme proposed for the Zn^{2+}/LOH system in methanol:water 95:5. The centrosymmetric isomer (2D) is taken as a reference for the energy level of the isomers. The complete nomenclature for each isomer is reported with, in parentheses, the energetically equivalent enantiomers.

Y_3 and Z_1, Z_2, Z_3 protons) belong to the $[Zn(LOH)_2]^{2+}$ structural isomers (2A−E). The two groups of protons Y_{1-3} and Z_{1-3} exchange with X, but there is no evidence of Y_{1-3} ↔ Z_{1-3} interconversion, i.e., Y_1, Y_2, and Y_3 exchange with each other but not with Z_{1-3}. This implies that $[Zn(LOH)Cl]^{+}$ is in equilibrium with two distinct sets of octahedral $[Zn(LOH)_2]^{2+}$ isomers (2A−C and 2D,E). To explain such a complexity, it has to be borne in mind that five octahedral isomers can be generated when using a racemic mixture of LOH as a consequence of the ligand and metal chirality (see Figure 9): three C_2-symmetric *RR*/*SS* isomers in enantiomeric pair (2A−C), a centrosymmetric *RS* isomer (2D, as found in the solid-state structure), and finally an *RS* asymmetric isomer (2E). According to their symmetry, 2A−D have to display a single set of signals, whereas 2E has to display two sets of signals. This would correspond to the six exchanging signals found in the EXSY at 300 K. DFT optimization of five $[Zn(LOH)_2]^{2+}$ model complexes was performed, and the relative energies were calculated by taking as a reference the centrosymmetric isomer 2D. The various molecular arrangements are too close in energy to provide information of a structural preference. In fact, the maximum energy difference of 6.3 kJ/mol (between 2A and 2B) is within the accuracy of the DFT calculation method[33,34] and would confirm that all five species can be present in solution in approximately equimolar ratio, in agreement with the NMR spectrum.

By means of quantitative EXSY analysis, the values of the exchange rate constants k_{ij}^{ex} (i = starting species/proton, j = derived species/proton) between the different pyridyl protons (X, Y_{1-3}, and Z_{1-3}) were obtained (Table 4). Since k_{ij}^{ex} are pseudo-first order, they can be compared, thus making speculations about the mechanisms of interconversion between various isomers, possible. It is evident that eight (underlined in Table 4) $[Zn(LOH)_2]^{2+}$ → $([Zn(LOH)_2]^{2+})^{\#}$ interconversions[35] (k_{ij}^{ex} 2.7(3)−0.45(2) s^{-1}) are faster than the $[Zn(LOH)Cl]^{+}$ → $[Zn(LOH)_2]^{2+}$ (0.06(2)−0.15(5) s^{-1}) and $[Zn(LOH)_2]^{2+}$ → $[Zn(LOH)Cl]^{+}$ (0.03(1)−0.07(2) s^{-1}) semi-reactions by approximately an order of magnitude. This would exclude the "dissociative/associative" pathway for interconversion of the octahedral species, $[Zn(LOH)_2][ZnCl_4]$ → $2[Zn(LOH)Cl]^{+} + 2Cl^{-}$ → $[Zn(LOH)_2]^{\#}[ZnCl_4]$, in favor of a rotational mechanism that would involve a ligand C_3

(33) Curtiss, L. A.; Raghavachari, K.; Redfern, P. C.; Pople, J. A. *Chem. Phys. Lett.* **1997**, *270*, 419−426.
(34) Curtiss, L. A.; Raghavachari, K.; Redfern, P. C.; Rassolov, V.; Pople, J. A. *J Chem. Phys.* **1998**, *109*, 7764−7776.
(35) # is used to distinguish two different interconverting octahedral isomers.

Scheme 6. First-Order (a) and Second-Order (b) Reaction Pathways Proposed for the Interconversion of the Different Zn^{2+}/LOH Species[a]

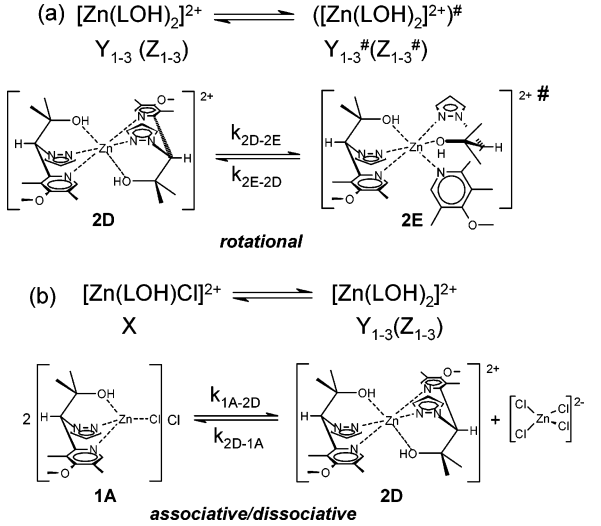

[a] X and $Y_{1-3}(Z_{1-3})$ correspond to $[Zn(LOH)Cl]^+$ and $[Zn(LOH)_2]^{2+}$ pyridyl protons, respectively. Selected examples are reported.

rotation around the $C_{chiral}-Zn-C_{chiral}$ axis with the transition state exhibiting a trigonal pyramidal geometry, Scheme 6. The other four interconversions $[Zn(LOH)_2]^{2+} \rightarrow ([Zn(LOH)_2]^{2+})^{\#}$ are slower (k_{ij}^{ex}: 0.11(8)−0.14(7) s^{-1}) and their k_{ij}^{ex} are comparable with those of the $[Zn(LOH)Cl]^+ \rightarrow [Zn(LOH)_2]^{2+}$ and $[Zn(LOH)_2]^{2+} \rightarrow [Zn(LOH)Cl]^+$ processes, making it difficult to discriminate between dissociative/associative or rotational mechanisms. This would signify that if the isomerization proceeds through a rotational mechanism, it would involve a considerably hindered trigonal prismatic transition state.

4. Conclusions

The heteroscorpionate 1-(4-methoxy-3,5-dimethyl-pyridin-2-yl)-2-methyl-1-pyrazol-1-yl-propan-2-ol (LOH) was synthesized in two high-yield steps. The ligand exhibits κ^3-N,N′,O coordination toward late transition divalent ions (M^{2+} = Ni^{2+}, Cu^{2+}, and Zn^{2+}) as evidenced by the X-ray structures of the complexes. Spectrophotometric (Cu^{2+} and Ni^{2+}) and ^1H NMR (Zn^{2+}) titrations provided further insight on the solution speciation and complexation constants, which are in accordance with the Irving−Williams series. Interestingly, in the solid state only octahedral centrosymmetric $[M(LOH)_2]^{2+}$ complexes were isolated also for 1:1 M^{2+}:LOH ratio. On the other hand, in solution there is evidence of 1:1 M^{2+}:LOH species. In the case of Zn^{2+}, $^1H-^1H$ EXSY spectroscopy revealed the occurrence of equilibria between different $[Zn(LOH)_2]^{2+}$ octahedral isomers and the $[Zn(LOH)Cl]^+$ tetrahedral species. Quantitative EXSY allowed determination of the rate constants of the different semi-reactions and proposal of two main interconversion pathways: (a) a rotational mechanism, which involves octahedral species interconversion (faster), and (b) a dissociative/associative mechanism, which involves octahedral−tetrahedral interconversion (slower). It is reasonable to assume that the presence of exchanging isomeric octahedral complexes in solution can be extended to the Ni^{2+} and Cu^{2+} systems even though we do not have direct evidence for it. As far as the LOH ligand is concerned, its versatile and easy two-step synthesis can be exploited for preparation of chiral N,N′,X-(Y)-tripodal donor ligands (X = O, S; Y = additional donor group as substituent on the pyrazole ring). We are currently investigating the synthesis and coordination properties of N,N′,S- and N,N′,S,S′-tripodal ligands prepared according to this procedure.

Acknowledgment. This work was supported by the Ministero dell'Istruzione, dell'Università e Ricerca (Rome, Italy).

Supporting Information Available: Crystal structures of **2a** and **5a** complexes; synthesis and crystal structure of $[Zn(L)Cl_2]\cdot$THF; spectrophotometric Ni^{2+}:LOH titration, NOESY/EXSY spectra of **5** at 300 and 250 K; semi-reaction rates r_{ij} and rate constant k_{ij} calculations. This material is available free of charge via the Internet at http://pubs.acs.org.

IC062228E